ORIGINAL ARTICLE

WILEY Cancer Science

Regulation of antitumor miR-144-5p targets oncogenes: Direct regulation of syndecan-3 and its clinical significance

Yasutaka Yamada[1,2] (iD) | Takayuki Arai[1,2] (iD) | Satoko Kojima[3] | Sho Sugawara[1,2] | Mayuko Kato[1,2] | Atsushi Okato[1,2] | Kazuto Yamazaki[4] | Yukio Naya[3] | Tomohiko Ichikawa[2] | Naohiko Seki[1]

[1]Department of Functional Genomics, Chiba University Graduate School of Medicine, Chiba, Japan

[2]Department of Urology, Chiba University Graduate School of Medicine, Chiba, Japan

[3]Department of Urology, Teikyo University Chiba Medical Center, Ichihara, Japan

[4]Department of Pathology, Teikyo University Chiba Medical Center, Ichihara, Japan

Correspondence: Naohiko Seki, Functional Genomics, Department of Functional Genomics, Chiba University Graduate School of Medicine, 1-8-1 Inohana Chuo-ku, Chiba 260-8670, Japan. (naoseki@faculty.chiba-u.jp).

In the human genome, *miR-451a*, *miR-144-5p* (passenger strand), and *miR-144-3p* (guide strand) reside in clustered microRNA (miRNA) sequences located within the 17q11.2 region. Low expression of these miRNAs is significantly associated with poor prognosis of patients with renal cell carcinoma (RCC) (*miR-451a*: $P = .00305$; *miR-144-5p*: $P = .00128$; *miR-144-3p*: $P = 9.45 \times 10^{-5}$). We previously reported that *miR-451a* acted as an antitumor miRNA in RCC cells. Involvement of the passenger strand of the *miR-144* duplex in the pathogenesis of RCC is not well understood. Functional assays showed that *miR-144-5p* and *miR-144-3p* significantly reduced cancer cell migration and invasive abilities, suggesting these miRNAs acted as antitumor miRNAs in RCC cells. Analyses of *miR-144-5p* targets identified a total of 65 putative oncogenic targets in RCC cells. Among them, high expression levels of 9 genes (*FAM64A*, *F2*, *TRIP13*, *ANKRD36*, *CENPF*, *NCAPG*, *CLEC2D*, *SDC3*, and *SEMA4B*) were significantly associated with poor prognosis ($P < .001$). Among these targets, expression of *SDC3* was directly controlled by *miR-144-5p*, and its expression enhanced cancer cell aggressiveness. We identified genes downstream by *SDC3* regulation. Data showed that expression of 10 of the downstream genes (*IL18RAP*, *SDC3*, *SH2D1A*, *GZMH*, *KIF21B*, *TMC8*, *GAB3*, *HLA-DPB2*, *PLEK*, and *C1QB*) significantly predicted poor prognosis of the patients ($P = .0064$). These data indicated that the antitumor *miR-144-5p*/oncogenic *SDC3* axis was deeply involved in RCC pathogenesis. Clustered miRNAs (*miR-451a*, *miR-144-5p*, and *miR-144-3p*) acted as antitumor miRNAs, and their targets were intimately involved in RCC pathogenesis.

KEYWORDS
antitumor, microRNA, *miR-144-5p*, renal cell carcinoma, SDC3

1 | INTRODUCTION

Renal cell carcinoma (RCC) is the most common form of adult kidney cancer. It accounts for approximately 3.8% of all newly diagnosed malignancies, and more than 140 000 people die worldwide every year.[1] Approximately 80% of RCC patients are classified with clear cell RCC.[2] Approximately 20%-30% of patients are found with advanced RCC at diagnosis, and the frequency of 5-year survival is only 12.1%. The treatment strategy of metastatic RCC remains confused.[3] Recently developed molecularly targeted therapeutics and immunotherapies have improved the prognosis of patients with advanced RCC, but recurrence, progression of distant metastasis,

and side-effects remain important issues associated with these treatments.[4] Searching for new therapeutic targets and developing useful prognostic markers are important issues to overcome in new treatments for RCC.

MicroRNAs (miRNAs), which are short, single-strand RNAs (19-22 nucleotides) belong to a group of noncoding RNA molecules that act as pivotal agents responsible for fine-tuning RNA expression in a sequence-dependent manner.[5] A vast number of studies have reported that miRNAs are closely involved in the physiological and pathological processes of disease.[6] In cancer cells, abnormal expression of miRNAs can disrupt regulatory networks and lead to cancer cell development, progression, metastasis, and drug resistance.[5,7,8] We have identified antitumor miRNAs (miR-10a-5p, miR-29s, miR-101, miR-149, and miR-451a) and their targets that are involved in the pathogenesis of RCC.[9-13] This strategy is a novel approach to identify new molecular targets and prognostic markers for RCC.

Previous miRNA biogenesis posits that the passenger strand of miRNA is degraded and does not regulate gene expression. Contrary to this concept, our miRNA expression signature of RCC showed that some miRNA passenger strands are aberrantly expressed in cancer tissues, for example, miR-139-3p, miR-144-5p, miR-145-3p, and miR-150-3p.[14-17] In fact, we found that some passenger strands actually act as antitumor miRNAs (miR-144-5p, miR-145-3p, miR-149-3p, miR-150-3p, and miR-199a-3p) through their targeting of oncogenes in several cancers.[12,15-19] These studies suggested the importance of analyzing passenger strands of miRNA duplex in cancer cells.

Our recent study showed that miR-451a was significantly downregulated in RCC tissues and acted as an antitumor miRNA in RCC cells.[13] Interestingly, miR-451a-regulated oncogenic targets were significantly associated with RCC pathogenesis.[13] In the human genome, miR-451a, miR-144-5p (the passenger strand), and miR-144-3p (the guide strand) are clustered together in chromosomal region 17q11.2. The Cancer Genome Atlas (TCGA) database analyses showed that low expression of miR-144-5p and miR-144-3p was significantly associated with poor prognosis of RCC patients ($P = .00128$ and $P = 9.45 \times 10^{-5}$, respectively).

In this study, we focused on miR-144-5p because the functional significance of miRNA passenger strands in RCC pathogenesis is obscure. Here, we studied the antitumor roles of miR-144-5p and identified the oncogenic targets involved in the pathogenesis of RCC. We suggest that identification of novel functions of miRNA passenger strands and the RNA networks they regulate might enhance our understanding of the molecular pathogenesis of RCC.

2 | MATERIALS AND METHODS

2.1 | Clinical RCC specimens and cell lines

We obtained a total of 18 clinical tissue specimens from RCC patients who underwent total nephrectomy at Chiba University Hospital (Chiba, Japan) between 2008 and 2015 (Table 1). All patients in our study provided signed informed consent, and the study protocol was approved by the Institutional Review Board of Chiba University (approval no. 484). We used 2 cell lines, 786-O and A498, obtained from ATCC (Manassas, VA, USA).

TABLE 1 Clinical features of 18 patients with clear cell renal cell carcinoma

No.	Age, years	Gender	Grade	pT	INF	v	ly	eg or ig	fc	im	rc	rp	s	Remarks
1	71	F	G2	T1a	a	0	0	eg	1	0	0	0	0	qRT-PCR
2	74	M	G1 > G2	T1a	a	0	0	eg	1	0	0	0	0	qRT-PCR
3	59	M	G3 > G2	T1b	a	0	0	eg	1	0	0	0	0	qRT-PCR
4	52	M	G2 > G3 > G1	T1a	a	0	0	eg	1	0	0	0	0	qRT-PCR
5	64	M	G2 > G3	T1b	a	0	0	eg	1	1	0	0	0	qRT-PCR
6	67	M	G2 > G3 > G1	T3a	b	1	0	ig	0	1	1	0	0	qRT-PCR
7	67	M	G2 > G3 > G1	T3a	b	1	0	ig	1	0	0	0	0	qRT-PCR
8	59	M	G3 > G2	T3a	b	1	0	ig	0	0	0	0	0	qRT-PCR
9	73	M	G1 > G3	T2a	a	0	1	eg	1	0	0	0	0	qRT-PCR
10	77	M	G1 > G2	T1b	a	0	0	eg	1	0	0	0	0	qRT-PCR
11	77	M	G2 > G1	T3a	a	1	0	eg	1	0	0	0	0	qRT-PCR
12	51	M	G2 > G1	T1b	a	0	0	eg	0	0	0	0	0	qRT-PCR
13	78	M	G2 > G1 > G3	T1b	b	0	0	eg	1	0	0	0	0	qRT-PCR
14	57	M	G1 > G2	T1a	a	0	0	eg	1	0	0	0	0	qRT-PCR
15	54	M	G2 > G1	T3a	a	0	0	eg	0	0	1	0	0	qRT-PCR
16	54	M	G1 > >G3	T2b	a	0	0	eg	1	0	0	0	0	qRT-PCR
17	74	F	G1 > G2	T2a	b	0	0	ig	1	0	0	0	0	qRT-PCR
18	65	M	G1 > G2	T1b	b	0	0	ig	1	0	0	0	0	IHC

a, clearly bounded with noncancer surrounding tissue; b, intermediate type; eg, expansive growth; F, female; fc, capsular formation; ig, infiltrative growth; IHC, immunohistochemistry; im, intrarenal metastasis; INF, infiltration; ly, lymph node; M, male; qRT-PCR, quantitative RT-PCR; rc, renal capsule invasion; rp, pelvis invasion; s, sinus invasion; v, vein.

2.2 | Transfection of mature miRNA and siRNA into RCC cells

The following RNA species were used in this study: mature miRNAs, pre-miR miRNA precursors (*hsa-miR-144-5p*, assay ID: PM12631; *hsa-miR-144-3p*, assay ID: PM11051; Applied Biosystems, Foster City, CA, USA), negative control miRNA (assay ID: AM 17111; Applied Biosystems), and siRNA (Stealth Select RNAi siRNA; si-*SDC3*, P/N: HSS145253 and HSS145254; Invitrogen, Carlsbad, CA, USA). The transfection methods were described previously.[11,20]

2.3 | Quantitative RT-PCR

The procedures for PCR quantification were described previously.[11,20] TaqMan probes and primers for *SDC3* (P/N:

Hs01568665_m1; Applied Biosystems) were assay-on-demand gene expression products. Quantitative RT-PCRs (qRT-PCRs) for *miR-144-5p* (P/N:002148; Applied Biosystems) and *miR-144-3p* (P/N:002676) were used to identify the expression levels of miRNAs according to the manufacturer's protocol. To normalize the data for quantification of mRNA and miRNAs, we used human *GAPDH* (P/N: Hs02786624_g1; Applied Biosystems), *GUSB* (P/N: Hs99999908_m1; Applied Biosystems), and *RNU48* (assay ID: 001006; Applied Biosystems).

2.4 | Cell proliferation, migration, and invasion assays

Cell proliferation abilities were determined by XTT assays using Cell Proliferation Kit II (Sigma-Aldrich, St. Louis, MO, USA). Cell migration was characterized with wound healing assays. Cell invasion abilities
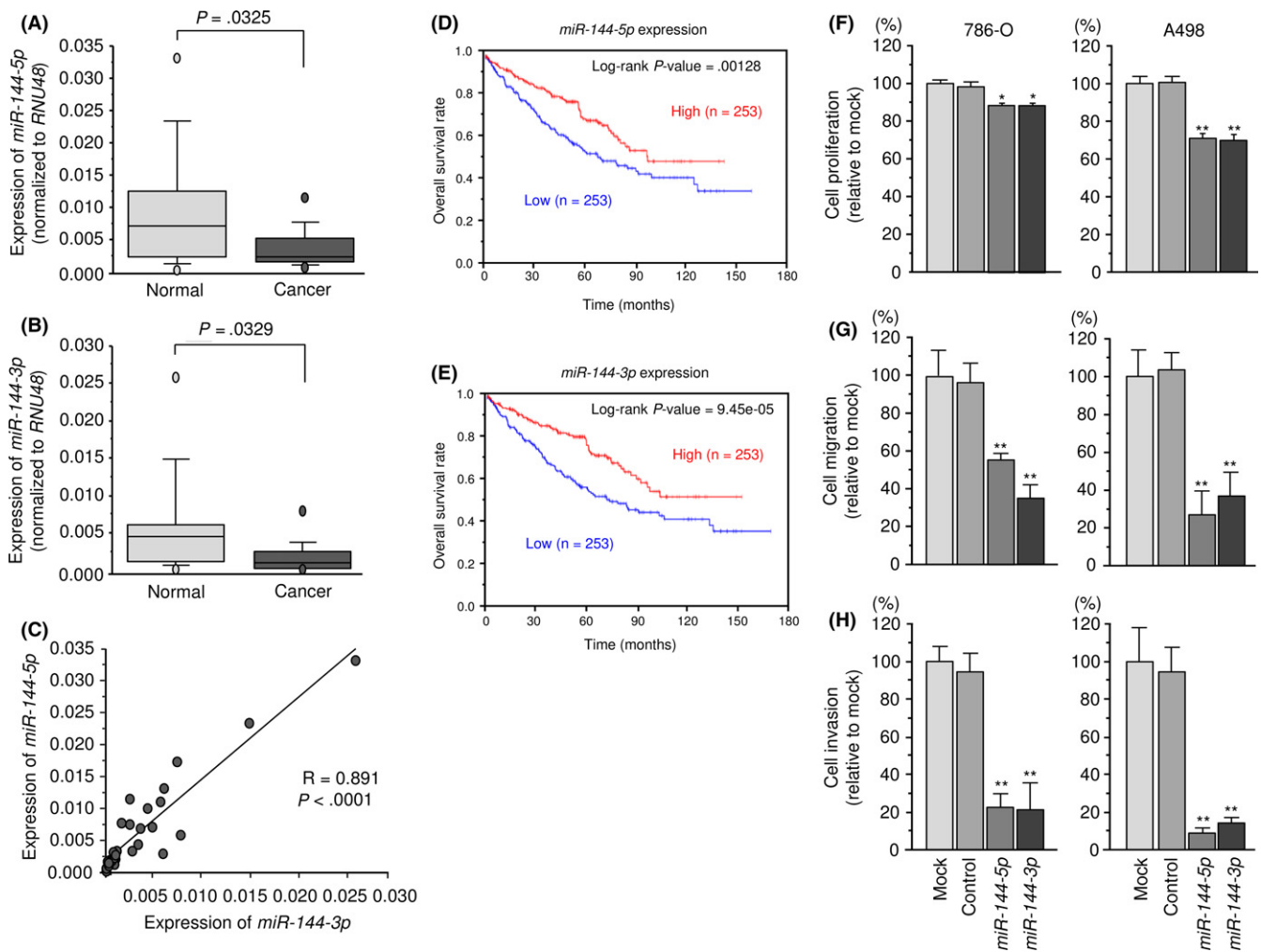
FIGURE 1 Expression levels, clinical significance, and functional roles of *miR-144-5p* and *miR-144-3p* in renal cell carcinoma (RCC). A-C, Expression levels of *miR-144-5p* and *miR-144-3p* in RCC clinical specimens. *RNU48* was used as an internal control. Spearman's rank test showed a positive correlation between the expression levels of *miR-144-5p* and *miR-144-3p*. D,E, From The Cancer Genome Atlas database, patients with low expression levels of either *miR-144-5p* or *miR-144-3p* had significantly reduced overall survival. F-H, Cell proliferation was determined by XTT assays. Cell migration activity was determined using migration assays. Cell invasion activity was determined using Matrigel invasion assays. *P < .005; **P < .0001

TABLE 2 miR-144-5p candidate target genes in renal cell carcinoma

Entrez gene ID	Gene symbol	Gene name	Site count	GEO expression data fold change (tumor/normal)	A498 miR-144-5p transfection (Log$_2$ ratio)	786-O miR-144-5p transfection (Log$_2$ ratio)	Average A498/786-O miR-144-5p transfection (Log$_2$ ratio)	Cytoband	TCGA data for OS (high vs low expression: P-value)
54478	FAM64A	Family with sequence similarity 64, member A	1	2.400	−1.290	−0.933	−1.111	hsj17p13.2	1.79E-07
2147	F2	Coagulation factor II (thrombin)	1	2.673	−0.234	−0.925	−0.579	hsj11p11.2	3.68E-07
9319	TRIP13	Thyroid hormone receptor interactor 13	1	2.551	−1.164	−0.652	−0.908	hsj5p15.33	9.70E-07
375248	ANKRD36	Ankyrin repeat domain 36	1	1.775	−0.874	−0.841	−0.857	hsj2q11.2	4.23E-05
1063	CENPF	Centromere protein F, 350/400 kDa	1	2.699	−0.717	−0.360	−0.539	hsj1q41	7.01E-05
64151	NCAPG	Non-SMC condensin I complex, subunit G	1	2.746	−1.624	−0.840	−1.232	hsj4p15.31	7.27E-05
29121	CLEC2D	C-type lectin domain family 2, member D	1	2.558	−1.014	−1.455	−1.235	hsj12p13.31	9.14E-05
9672	SDC3	Syndecan 3	1	2.432	−0.894	−0.977	−0.936	hsj1p35.2	0.000271
10509	SEMA4B	Sema domain, immunoglobulin domain (Ig), transmembrane domain (TM) and short cytoplasmic domain, (semaphorin) 4B	1	2.298	−0.692	−0.934	−0.813	hsj15q26.1	0.000821
81552	VOPP1	Vesicular, overexpressed in cancer, prosurvival protein 1	1	1.842	−0.406	−1.035	−0.720	hsj7p11.2	0.004190
727936	GXYLT2	Glucoside xylosyltransferase 2	3	2.640	−0.590	−0.814	−0.702	hsj3p13	0.004620
3832	KIF11	Kinesin family member 11	1	2.461	−1.241	−1.236	−1.238	hsj10q23.33	0.004640
29028	ATAD2	ATPase family, AAA domain containing 2	1	2.606	−0.844	−0.507	−0.676	hsj8q24.13	0.006000
3090	HIC1	Hypermethylated in cancer 1	1	2.709	−0.994	−0.022	−0.508	hsj17p13.3	0.009480
51060	TXNDC12	Thioredoxin domain containing 12 (endoplasmic reticulum)	1	1.579	−0.564	−0.765	−0.665	hsj1p32.3	0.009760
710	SERPING1	Serpin peptidase inhibitor, clade G (C1 inhibitor), member 1	1	2.015	−0.558	−0.536	−0.547	hsj11q12.1	0.016900
59345	GNB4	Guanine nucleotide-binding protein (G protein), beta polypeptide 4	1	1.862	−0.881	−1.421	−1.151	hsj3q26.33	0.053200
1356	CP	Ceruloplasmin (ferroxidase)	1	15.420	−1.753	−1.380	−1.566	hsj3q24	0.070000
5272	SERPINB9	Serpin peptidase inhibitor, clade B (ovalbumin), member 9	1	1.797	−0.462	−1.730	−1.096	hsj6p25.2	0.078200
5046	PCSK6	Proprotein convertase subtilisin/kexin type 6	1	7.374	−0.930	−1.827	−1.379	hsj15q26.3	0.080000
586	BCAT1	Branched chain amino acid transaminase 1, cytosolic	2	3.076	−0.850	−1.324	−1.087	hsj12p12.1	0.100000
54437	SEMA5B	Sema domain, seven thrombospondin repeats (type 1 and type 1-like), transmembrane domain (TM) and short cytoplasmic domain, (semaphorin) 5B	1	7.089	−0.706	−2.687	−1.696	hsj3q21.1	0.109000
317	APAF1	Apoptotic peptidase activating factor 1	1	1.839	−0.973	−1.014	−0.994	hsj12q23.1	0.121000
10718	NRG3	Neuregulin 3	1	1.977	−1.645	−0.389	−1.017	hsj10q23.1	0.213000
51316	PLAC8	Placenta-specific 8	2	2.750	−0.630	−1.962	−1.296	hsj4q21.22	0.249000
7436	VLDLR	Very low density lipoprotein receptor	1	2.186	−0.455	−0.817	−0.636	hsj9p24.2	0.254000
1050	CEBPA	CCAAT/enhancer binding protein (C/EBP), alpha	1	1.531	−0.877	−0.648	−0.763	hsj19q13.11	0.320000
64919	BCL11B	B-cell CLL/lymphoma 11B (zinc finger protein)	1	2.484	−0.178	−1.121	−0.649	hsj14q32.2	0.340000

(Continues)

TABLE 2 (Continued)

Entrez gene ID	Gene symbol	Gene name	Site count	GEO expression data fold change (tumor/normal)	A498 miR-144-5p transfection (Log$_2$ ratio)	786-O miR-144-5p transfection (Log$_2$ ratio)	Average A498/786-O miR-144-5p transfection (Log$_2$ ratio)	Cytoband	TCGA data for OS (high vs low expression: P-value)
56950	SMYD2	SET and MYND domain containing 2	1	1.657	−0.501	−0.762	−0.631	hs|1q41	0.343000
11096	ADAMTS5	ADAM metallopeptidase with thrombospondin type 1 motif, 5	2	1.523	−0.188	−0.946	−0.567	hs|21q21.3	0.394000
1009	CDH11	Cadherin 11, type 2, OB-cadherin (osteoblast)	1	1.848	−0.792	−1.789	−1.290	hs|16q21	0.426000
149628	PYHIN1	Pyrin and HIN domain family, member 1	1	1.968	−1.154	−1.032	−1.093	hs|1q23.1	0.474000
27010	TPK1	Thiamin pyrophosphokinase 1	1	1.578	−0.810	−0.591	−0.701	hs|7q35	0.487000
8357	HIST1H3H	Histone cluster 1, H3 h	1	3.446	−0.690	−1.521	−1.105	hs|6p22.1	0.516000
4082	MARCKS	Myristoylated alanine-rich protein kinase C substrate	2	2.769	−1.310	−2.252	−1.781	hs|6q21	0.528000
23468	CBX5	Chromobo x homolog 5	2	1.659	−1.157	−1.216	−1.187	hs|12q13.13	0.549000
79627	OGFRL1	Opioid growth factor receptor-like 1	2	2.107	−0.940	−0.167	−0.553	hs|6q13	0.587000
571	BACH1	BTB and CNC homology 1, basic leucine zipper transcription factor 1	1	1.649	−0.197	−1.127	−0.662	hs|21q21.3	0.622000
23102	TBC1D2B	TBC1 domain family, member 2B	1	1.654	−0.974	−0.531	−0.752	hs|15q24.3	0.693000
4481	MSR1	Macrophage scavenger receptor 1	1	2.887	−1.581	−1.135	−1.358	hs|8p22	0.705000
493	ATP2B4	ATPase, Ca++ transporting, plasma membrane 4	1	2.282	−1.285	−0.928	−1.106	hs|1q32.1	0.723000
56124	PCDHB12	Protocadherin beta 12	1	2.095	−0.179	−0.844	−0.512	hs|5q31.3	0.765000
3556	IL1RAP	Interleukin 1 receptor accessory protein	1	1.775	−0.170	−1.024	−0.597	hs|3q28	0.774000
9201	DCLK1	Doublecortin-like kinase 1	1	3.633	−1.282	−0.906	−1.094	hs|13q13.3	0.804000
488	ATP2A2	ATPase, Ca++ transporting, cardiac muscle, slow twitch 2	1	1.522	−1.297	−0.891	−1.094	hs|12q24.11	0.816000
9545	RAB3D	RAB3D, member RAS oncogene family	1	1.956	−1.106	−0.074	−0.590	hs|19p13.2	0.846000
4330	MN1	Meningioma (disrupted in balanced translocation) 1	1	1.682	−0.170	−0.855	−0.512	hs|22q12.1	0.846000
23036	ZNF292	Zinc finger protein 292	2	2.177	−0.792	−0.573	−0.683	hs|6q14.3	0.900000
9770	RASSF2	Ras association (RalGDS/AF-6) domain family member 2	1	6.147	−1.030	−0.058	−0.544	hs|20p13	0.911000
11120	BTN2A1	Butyrophilin, subfamily 2, member A1	1	1.520	−1.328	−0.533	−0.930	hs|6p22.2	0.912000
11237	RNF24	Ring finger protein 24	1	1.606	−0.831	−0.578	−0.704	hs|20p13	0.918000
23023	TMCC1	Transmembrane and coiled-coil domain family 1	1	4.679	−0.791	−0.349	−0.570	hs|3q22.1	0.945000
636	BICD1	Bicaudal D homolog 1 (Drosophila)	1	2.423	−0.557	−0.590	−0.574	hs|12p11.21	0.955000
6424	SFRP4	Secreted frizzled-related protein 4	1	1.786	−1.625	−1.025	−1.325	hs|7p14.1	0.980000
54769	DIRAS2	DIRAS family, GTP-binding RAS-like 2	3	6.202	−0.204	−2.678	−1.441	hs|9q22.2	0.001190[a]
196	AHR	Aryl hydrocarbon receptor	1	1.745	−0.816	−1.261	−1.039	hs|7p21.1	0.011700[a]
283	ANG	Angiogenin, ribonuclease, RNase A family, 5	2	1.617	−0.554	−0.906	−0.730	hs|14q11.2	0.015300[a]
8490	RGS5	Regulator of G protein signaling 5	1	4.721	−0.938	−0.705	−0.821	hs|1q23.3	0.031700[a]

(Continues)

TABLE 2 (Continued)

Entrez gene ID	Gene symbol	Gene name	Site count	GEO expression data fold change (tumor/normal)	A498 miR-144-5p transfection (Log$_2$ ratio)	786-O miR-144-5p transfection (Log$_2$ ratio)	Average A498/786-O miR-144-5p transfection (Log$_2$ ratio)	Cytoband	TCGA data for OS for high vs low expression: P-value
54941	RNF125	Ring finger protein 125, E3 ubiquitin protein ligase	1	1.527	−0.789	−0.321	−0.555	hs|18q12.1	0.038200[a]
80854	SETD7	SET domain containing (lysine methyltransferase) 7	1	2.225	−0.662	−0.854	−0.758	hs|4q31.1	0.045900[a]
81575	APOLD1	Apolipoprotein L domain containing 1	1	3.953	−1.531	−1.101	−1.316	hs|12p13.1	2.21E−06[a]
143872	ARHGAP42	Rho GTPase activating protein 42	1	2.075	−1.289	−1.614	−1.452	hs|11q22.1	4.85E−05[a]
642273	FAM110C	Family with sequence similarity 110, member C	1	2.149	−1.376	−0.041	−0.708	hs|2p25.3	5.9E−06[a]
375287	RBM43	RNA binding motif protein 43	1	1.630	−0.377	−0.994	−0.685	hs|2q23.3	6.29E−05[a]
4601	MXI1	MAX interactor 1, dimerization protein	1	1.987	−1.649	−0.513	−1.081	hs|10q25.2	9.79E−05[a]

[a]Poor prognosis with low gene expression.

GEO, Gene Expression Omnibus; OS, overall survival; TCGA, The Cancer Genome Atlas.

were determined with modified Boyden chambers containing Transwell-precoated Matrigel membrane filter inserts.[11,20]

2.5 | Incorporation of miR-144-5p or miR-144-3p into the RNA-induced silencing complex by Ago2 immunoprecipitation

786-O cells were transfected with 10 nmol/L miRNAs by reverse transfection. After 48 hours, immunoprecipitation was carried out using a human AGO2 miRNA isolation kit (Wako, Osaka, Japan).[16] Expression levels of *miR-144-5p* or *miR-144-3p* were evaluated by qRT-PCR. MicroRNA data were normalized to the expression of *miR-26a* (P/N:000405; Applied Biosystems), which was not influenced by *miR-144-5p* or *miR-144-3p* transfection.

2.6 | Western blot analysis

Immunoblotting was carried out with monoclonal anti-SDC3 antibodies (1:400 dilution; SAB4301620; Sigma-Aldrich). We used anti-GAPDH antibodies (1:10 000 dilution; ab8245; Abcam, Cambridge, UK) as an internal control.[11,20]

2.7 | Identification of candidate genes regulated by *miR-144-5p* and *miR-144-3p* in RCC cells

Candidate genes regulated by *miR-144-5p* and *miR-144-3p* were identified by a combination of in silico and genomewide gene expression analyses. Genes possessing sequences regulated by *miR-144-5p* and *miR-144-3p* were obtained from the TargetScan database (http://www.targetscan.org/vert_71/). Upregulated genes in RCC were identified from publicly available datasets in the Gene Expression Omnibus (GEO; accession no. GSE36895) and we narrowed down the candidate genes as explained below. Oligo microarrays (Human GE 60K; Agilent Technologies, Santa Clara, CA, USA) were used for gene expression analyses. The microarray data were deposited into GEO (http://www.ncbi.nlm.nih.gov/geo/), with accession number GSE106791. The Genomics Analysis and Visualization Platform was used for visualization of gene expression heat maps and clustering.[21] The normalized mRNA expression values in the RNA sequencing data were processed and provided as Z scores. In the present study, patients were divided into two groups: Z-score $\geq$ 0 and Z-score < 0.

2.8 | Plasmid construction and dual-luciferase reporter assay

The partial wild-type sequence of the *SDC3* 3′-UTR was inserted between the *Sgf*I-*Pme*I restriction sites in the 3′-UTR of the h*Rluc* gene in the psiCHECK-2 vector (C8021; Promega, Madison, WI, USA). We used sequences that were missing the *miR-144-5p* target sites (position 2166-2172). The synthesized DNA was cloned into the psiCHECK-2 vector.[11,20]

TABLE 3 *miR-144-3p* candidate target genes in renal cell carcinoma

Entrez gene ID	Gene symbol	Gene name	Conserved site count	Poorly conserved site count	GEO expression data fold change (tumor/normal)	A498 miR-144-3p transfection (Log$_2$ ratio)	786-O miR-144-3p transfection (Log$_2$ ratio)	Average A498/786-O miR-144-3p transfection (Log$_2$ ratio)	Cytoband	TCGA data for OS (high vs low expression: P-value)
5373	PMM2	Phosphomannomutase 2	1	0	1.580	−1.617	−1.020	−1.319	hsa|16p13.2	2.18E-07
55165	CEP55	Centrosomal protein 55 kDa	1	1	4.202	−1.743	−1.130	−1.437	hsa|10q23.33	6.94E-07
79733	E2F8	E2F transcription factor 8	1	0	4.133	−0.537	−0.722	−0.630	hsa|11p15.1	0.00145
9134	CCNE2	Cyclin E2	1	0	2.430	−0.591	−1.823	−1.207	hsa|8q22.1	0.00664
23657	SLC7A11	Solute carrier family 7 (anionic amino acid transporter light chain, xc- system), member 11	1	5	2.678	−0.418	−1.195	−0.806	hsa|4q28.3	0.02340
1462	VCAN	Versican	1	1	5.753	−0.695	−0.883	−0.789	hsa|5q14.3	0.04670
2335	FN1	Fibronectin 1	1	1	5.453	−1.470	−0.105	−0.787	hsa|2q35	0.07790
5738	PTGFRN	Prostaglandin F2 receptor inhibitor	1	0	2.242	−0.565	−0.981	−0.773	hsa|1p13.1	0.08260
57561	ARRDC3	Arrestin domain containing 3	1	2	1.705	−0.381	−0.940	−0.660	hsa|5q14.3	0.11100
11116	FGFR1OP	FGFR1 oncogene partner	1	1	1.551	−0.499	−0.881	−0.690	hsa|6q27	0.17000
7436	VLDLR	Very low density lipoprotein receptor	1	2	2.186	−0.455	−0.817	−0.636	hsa|9p24.2	0.25400
1050	CEBPA	CCAAT/enhancer binding protein (C/EBP), alpha	1	0	1.531	−0.877	−0.648	−0.763	hsa|19q13.11	0.32000
4154	MBNL1	Muscleblind-like splicing regulator 1	3	0	1.743	−0.610	−0.947	−0.779	hsa|3q25.2	0.32100
64919	BCL11B	B-cell CLL/lymphoma 11B (zinc finger protein)	1	0	2.484	−0.178	−1.121	−0.649	hsa|14q32.2	0.34000
11096	ADAMTS5	ADAM metallopeptidase with thrombospondin type 1 motif, 5	1	2	1.523	−0.188	−0.946	−0.567	hsa|21q21.3	0.39400
1009	CDH11	Cadherin 11, type 2, OB-cadherin (osteoblast)	1	0	1.848	−0.792	−1.789	−1.290	hsa|16q21	0.42600
3796	KIF2A	Kinesin heavy chain member 2A	1	2	2.008	−0.922	−1.005	−0.963	hsa|5q12.1	0.44500
55205	ZNF532	Zinc finger protein 532	1	0	1.899	−0.790	−1.560	−1.175	hsa|18q21.32	0.50400
4082	MARCKS	Myristoylated alanine-rich protein kinase C substrate	1	1	2.769	−1.310	−2.252	−1.781	hsa|6q21	0.52800
79627	OGFRL1	Opioid growth factor receptor-like 1	1	2	2.107	−0.940	−0.167	−0.553	hsa|6q13	0.58700
22795	NID2	Nidogen 2 (osteonidogen)	1	0	1.527	−0.935	−0.208	−0.571	hsa|14q22.1	0.62800
2200	FBN1	Fibrillin 1	2	0	2.173	−0.605	−1.049	−0.827	hsa|15q21.1	0.63000
10957	PNRC1	Proline-rich nuclear receptor coactivator 1	1	0	1.724	−0.640	−0.875	−0.757	hsa|6q15	0.72000
79365	BHLHE41	Basic helix-loop-helix family, member e41	1	2	9.461	−0.947	−0.568	−0.758	hsa|12p12.1	0.89500
23036	ZNF292	Zinc finger protein 292	1	1	2.177	−0.792	−0.573	−0.683	hsa|6q14.3	0.90000
23023	TMCC1	Transmembrane and coiled-coil domain family 1	1	0	4.679	−0.791	−0.349	−0.570	hsa|3q22.1	0.94500

(Continues)

TABLE 3 (Continued)

Entrez gene ID	Gene symbol	Gene name	Conserved site count	Poorly conserved site count	GEO expression data fold change (tumor/normal)	A498 miR-144-3p transfection (Log$_2$ ratio)	786-O miR-144-3p transfection (Log$_2$ ratio)	Average A498/786-O miR-144-3p transfection (Log$_2$ ratio)	Cytoband	TCGA data for OS (high vs low expression): P-value
4131	MAP1B	Microtubule-associated protein 1B	1	0	2.795	−0.448	−0.880	−0.664	hs|5q13.2	0.99300
8445	DYRK2	Dual-specificity tyrosine-(Y)-phosphorylation regulated kinase 2	2	0	1.729	−0.494	−0.518	−0.506	hs|12q15	0.000356[a]
1003	CDH5	Cadherin 5, type 2 (vascular endothelium)	1	0	2.616	−0.439	−0.643	−0.541	hs|16q21	0.00935[a]
23097	CDK19	Cyclin-dependent kinase 19	1	2	2.174	−0.145	−0.891	−0.518	hs|6q21	0.01660[a]
2908	NR3C1	Nuclear receptor subfamily 3, group C, member 1 (glucocorticoid receptor)	1	0	2.111	−0.667	−1.105	−0.886	hs|5q31.3	0.01780[a]
54492	NEURL1B	Neuralized E3 ubiquitin protein ligase 1B	1	0	2.907	−0.637	−0.810	−0.723	hs|5q35.1	0.03430[a]
54941	RNF125	Ring finger protein 125, E3 ubiquitin protein ligase	1	1	1.527	−0.789	−0.321	−0.555	hs|18q12.1	0.03820[a]
114800	CCDC85A	Coiled-coil domain containing 85A	1	0	2.334	−1.409	−0.189	−0.799	hs|2p16.1	3.69E-05[a]

[a]Poor prognosis with low gene expression.
GEO, Gene Expression Omnibus; OS, overall survival; TCGA, The Cancer Genome Atlas.

2.9 | Immunohistochemistry

Tissue sections were incubated overnight at 4°C with anti-SDC3 antibodies diluted 1:50 (SAB4301620; Sigma-Aldrich).[11,20]

2.10 | Regulation of targets downstream of SDC3 in RCC

We further investigated pathways regulated by *SDC3* in RCC cells. We analyzed gene expression using si-*SDC3*-transfected 786-O cells. Microarray data were used for expression profiling of si-*SDC3* transfectants. The microarray data were deposited into GEO (accession no. GSE113066).

2.11 | Clinical data analysis based on TCGA datasets

To investigate the clinical significance of miRNAs and genes in RCC, we used the RNA sequence database in TCGA (https://tcga-data.nci.nih.gov/tcga/). The gene expression and clinical data were obtained from cBioPortal (http://www.cbioportal.org/, the provisional data downloaded on 1 December 2017).[22-24]

2.12 | Statistical analysis

Relationships between 2 or 3 variables and numerical values were analyzed with Mann-Whitney *U* tests or Bonferroni-adjusted Mann-Whitney *U*-tests. Spearman's rank tests were used to analyze the correlations of the expressions. Expert StatView software (version 5.0; SAS Institute, Cary, NC, USA) was used for these analyses. Univariate and multivariate Cox proportional hazard regression models were used to determine prognostic factors with JMP Pro 13 (SAS Institute Inc., Cary, NC, USA).

3 | RESULTS

3.1 | Expression levels of *miR-144-5p* and *miR-144-3p* in RCC clinical specimens

As shown in Figure 1, the expression levels of *miR-144-5p* and *miR-144-3p* were significantly lower in cancer tissues compared with those in adjacent noncancerous tissues ($P = .0325$ and $P = .0329$, respectively; Figure 1A,B). Furthermore, Spearman's rank test showed a positive correlation between the expression levels of *miR-144-5p* and *miR-144-3p* in clinical specimens ($R = 0.891$, $P < .0001$; Figure 1C).

3.2 | Clinical significance and functional roles of miR-144-5p and miR-144-3p in RCC

From TCGA database, patients with low expression levels of both *miR-144-5p* and *miR-144-3p* were significantly associated with poor prognosis ($P = .00128$ and $P = 9.45 \times 10^{-5}$, respectively; Figure 1D,E).

We undertook gain-of-function assays using miRNA transfection into two RCC cell lines. Ectopic expression of *miR-144-5p* and *miR-144-3p* showed that both *miR-144-5p* and *miR-144-3p* reduced cancer cell proliferation, migration, and invasive abilities in comparison with mock and miR-control transfectants (Figure 1F-H).

3.3 | Incorporation of miR-144-5p into the RNA-induced silencing complex in RCC cells

We carried out immunoprecipitation with antibodies targeting Ago2, which plays a pivotal role in the RNA-induced silencing complex (RISC). After transfection with *miR-144-5p* and immunoprecipitation by anti-Ago2 antibodies, *miR-144-5p* levels were significantly higher than those of mock- or miR-control-transfected cells or those of *miR-144-3p*-transfected 786-O cells ($P < .0001$; Figure S1A). Similarly, after *miR-144-3p* transfection, *miR-144-3p* was detected by Ago2 immunoprecipitation ($P < .0001$; Figure S1B).

3.4 | Identification of candidate targets of miR-144-5p and miR-144-3p regulation in RCC cells

We searched for candidate targets using a combination of genome-wide gene expression and in silico database analyses. The strategy for identification of *miR-144-5p* and *miR-144-3p* target genes is shown in Figure S2. First, we identified 2078 and 1043 genes that had putative target sites for *miR-144-5p* and *miR-144-3p*, respectively in their 3′-UTRs based upon the TargetScanHuman 7.1

database. Next, we narrowed down those presumptive targets to 227 and 268 genes, respectively based on expression levels that were upregulated (fold change >1.5) in RCC tissues using the GEO database. Next, we identified 65 and 34 genes that were downregulated after *miR-144-5p* and *miR-144-3p* transfection, respectively into RCC cells (Log_2 ratio < -0.5; Tables 2,3). In this study, we focused on *miR-144-5p*, the passenger strand of the *miR-144* duplex. As shown in Figure 2, 65 candidate target genes of *miR-144-5p* were analyzed, allowing us to construct a heat map. Among those genes, 9 were significantly associated with poor prognosis in RCC patients ($P < .001$; Figure 3). Heat map visualization of those genes is shown in Figure 4A. Patients with high gene signature expression (Z-score ≥ 0) had poorer outcomes (disease-free survival and overall survival) than those with low gene signature expression (Z-score < 0) ($P < .0001$; Figure 4B,C). In the present study, we focused on syndecan-3 (*SDC3*), reportedly related to carcinogenesis in several types of cancers.

3.5 | Direct regulation of SDC3 by miR-144-5p in RCC cells

We asked whether the expression of the *SDC3* gene and SDC3 protein decreased in *miR-144-5p*-transfected RCC cells. As shown in Figure 5A,B, both mRNA and protein levels were significantly decreased by *miR-144-5p* transfection compared with the mock, miR-control, or *miR-144-3p* transfectants.

Next, luciferase reporter assays with a vector that included the 3′-UTR of *SDC3* were undertaken to confirm that *miR-144-*
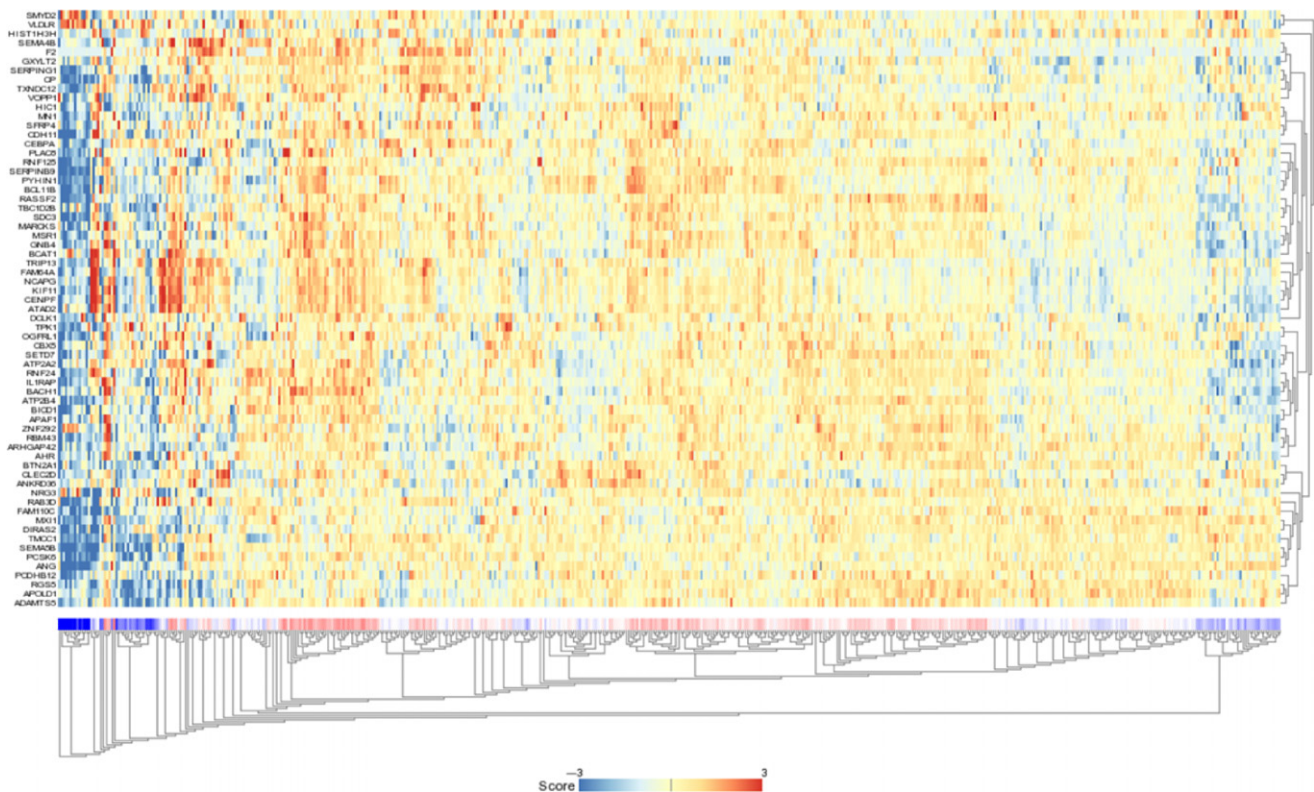
FIGURE 2 Heat map showing the expression of 65 genes targeted by *miR-144-5p*

5p directly regulated *SDC3* in a sequence-dependent manner. The TargetScanHuman database predicted that there was a binding site for *miR-144-5p* in the 3′-UTR of *SDC3* (position 2166-2172; Figure 5C). Cotransfection with *miR-144-5p* and vectors significantly decreased luciferase activity in comparison with those in mock and miR-control transfectants (Figure 5D).

## 3.6 | Effects of silencing *SDC3* on cell proliferation, migration, and invasion in RCC cells

We confirmed that the expression levels of *SDC3* mRNA and SDC3 protein were decreased by si-*SDC3* in RCC cells (Figure 6A,B). Furthermore, we investigated the effects of silencing *SDC3* on cell proliferation, migration, and invasion in RCC cells. Cancer aggressiveness was significantly inhibited in si-*SDC3* transfectants in comparison with that in mock- or miR-control-transfected cell lines (Figure 6C-E).

3.7 | Expression of SDC3 in RCC clinical specimens

We examined the mRNA expression levels of *SDC3* in 17 RCC clinical specimens using qRT-PCR. The mRNA expression levels of *SDC3* were significantly upregulated in cancer tissues compared with those in adjacent noncancerous tissues (Figure 7A). Spearman's rank test revealed a negative correlation between the expression of *SDC3* and *miR-144-5p* (P = .0409, R = −0.356, Figure 7B). Next, we investigated the expression levels of SDC3 in RCC clinical specimens by immunostaining. It was found that SDC3 was strongly overexpressed in several cancer lesions compared with that in adjacent noncancerous lesions with the same staining intensity (Figure 7C).

## 3.8 | Downstream genes affected by silencing of *SDC3* in RCC cells

Finally, we undertook a genomewide gene expression analysis using si-*SDC3*-treated 786-O cells to investigate which genes were modulated
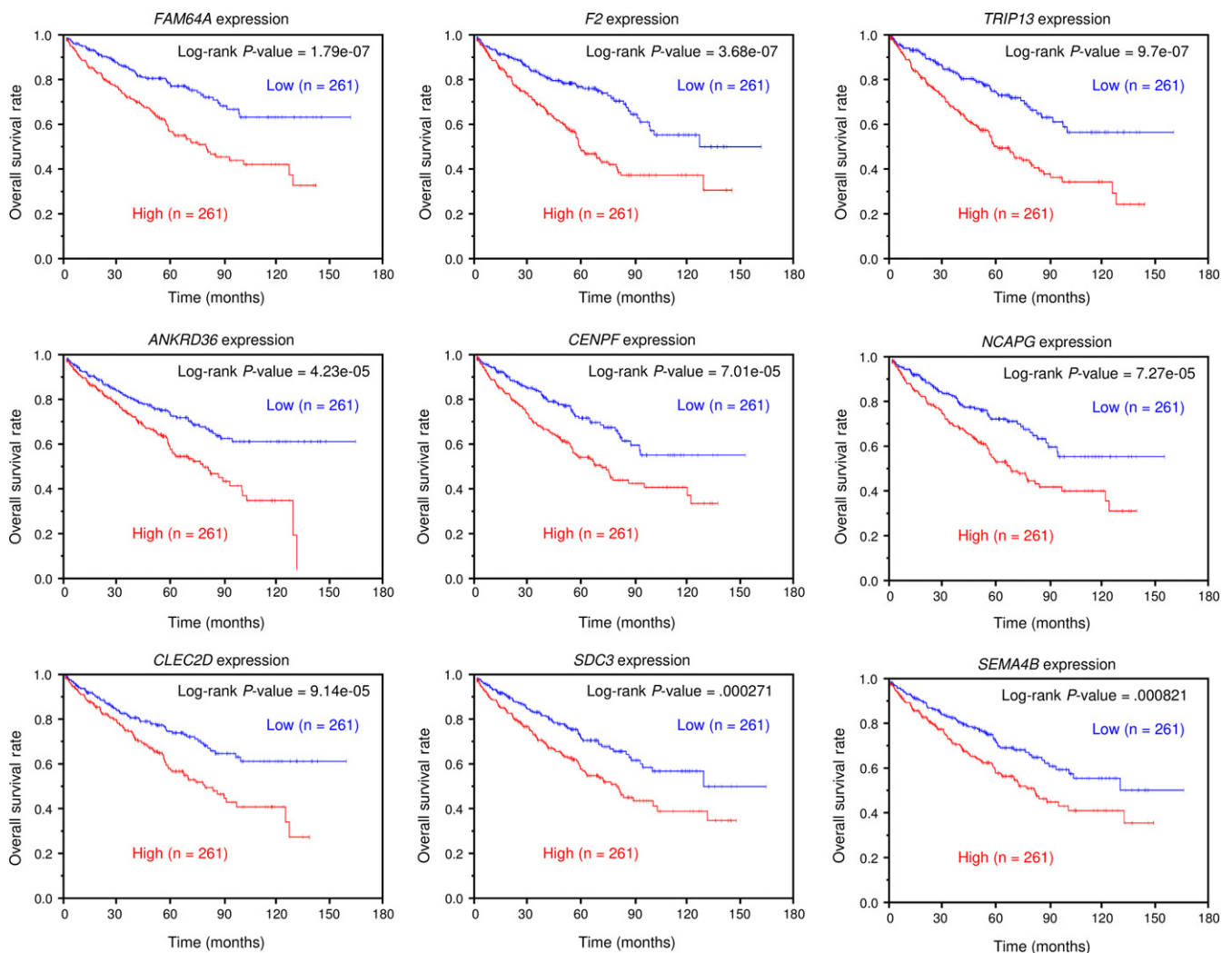
FIGURE 3 The Cancer Genome Atlas database analysis of putative targets of *miR-144-5p* in renal cell carcinoma. Kaplan-Meier plots of overall survival with log-rank tests for 9 genes regulated by *miR-144-5p* with high and low gene expression from The Cancer Genome Atlas database
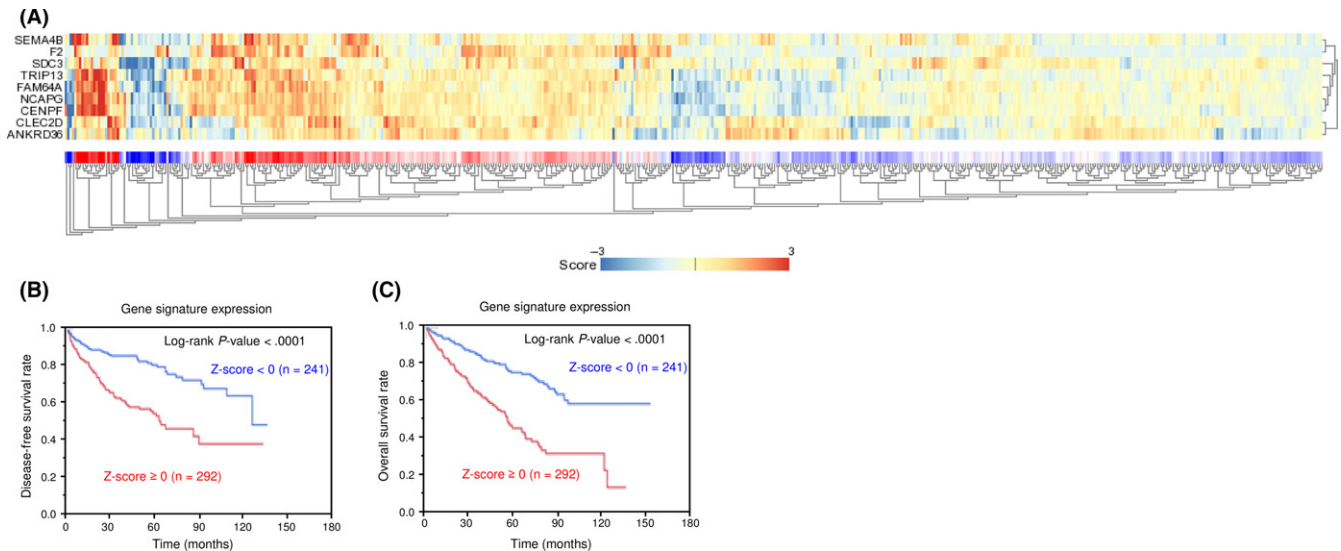
FIGURE 4 Heat map showing gene expression and Kaplan-Meier analysis of 9 candidate genes in renal cell carcinoma. A, Heat map visualization of 9 candidate genes. B, Kaplan-Meier analysis of disease-free survival of patients with high gene signature expression and those with a low gene signature expression. C, Kaplan-Meier analysis of overall survival of patients with high gene signature expression and those with a low gene signature expression
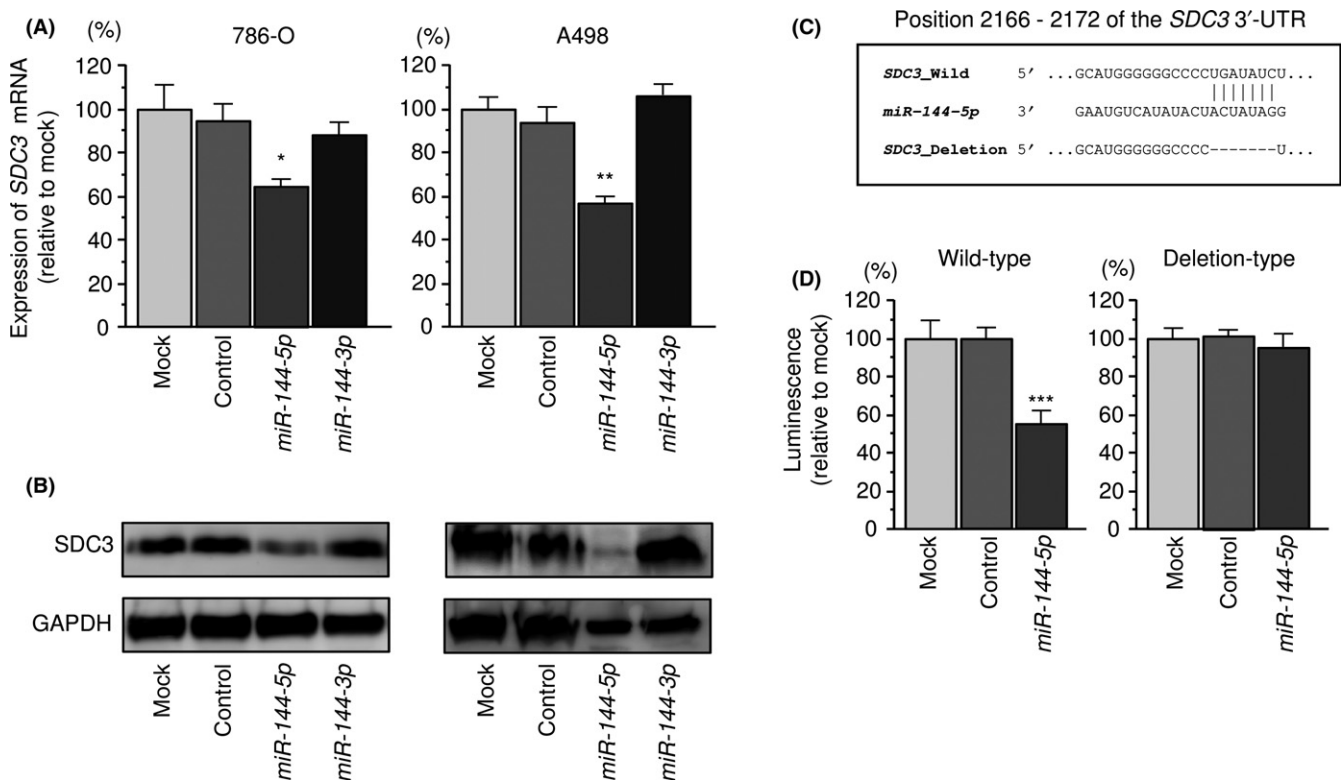
FIGURE 5 Regulation of *SDC3* expression by *miR-144-5p* in renal cell carcinoma cells. A, Expression levels of *SDC3* mRNA 48 hours after transfection with 10 nmol/L *miR-144-5p* or *miR-144-3p* into cell lines. *GAPDH* was used as an internal control. *$P < .0001$. B, Protein expression of syndecan-3 (SDC3) 72 hours after transfection with *miR-144-5p* or *miR-144-3p*. GAPDH was used as a loading control. C, *miR-144-5p* binding sites in the 3′-UTR of *SDC3* mRNA. D, Dual-luciferase reporter assays using vectors encoding putative *miR-144-5p* target sites (positions 2166-2172) in the *SDC3* 3′-UTR for both wild-type and deletion-type. Normalized data were calculated as the ratio of *Renilla*/firefly luciferase activities. *$P < .005$; **$P < .001$; ***$P < .05$

by *SDC3*. A SurePrint G3 Human GE 60K v3 microarray (Agilent Technologies) was used for genomewide expression analysis. We focused on genes that were significantly downregulated by transfection of both si-

*SDC3*_1 and si-*SDC3*_2 ($\log_2$ [average-si-*SDC3*/mock] < -1.0). *SDC3* was the most significantly downregulated gene, indicating that the array data were worthy of evaluation. We identified 26 candidate genes
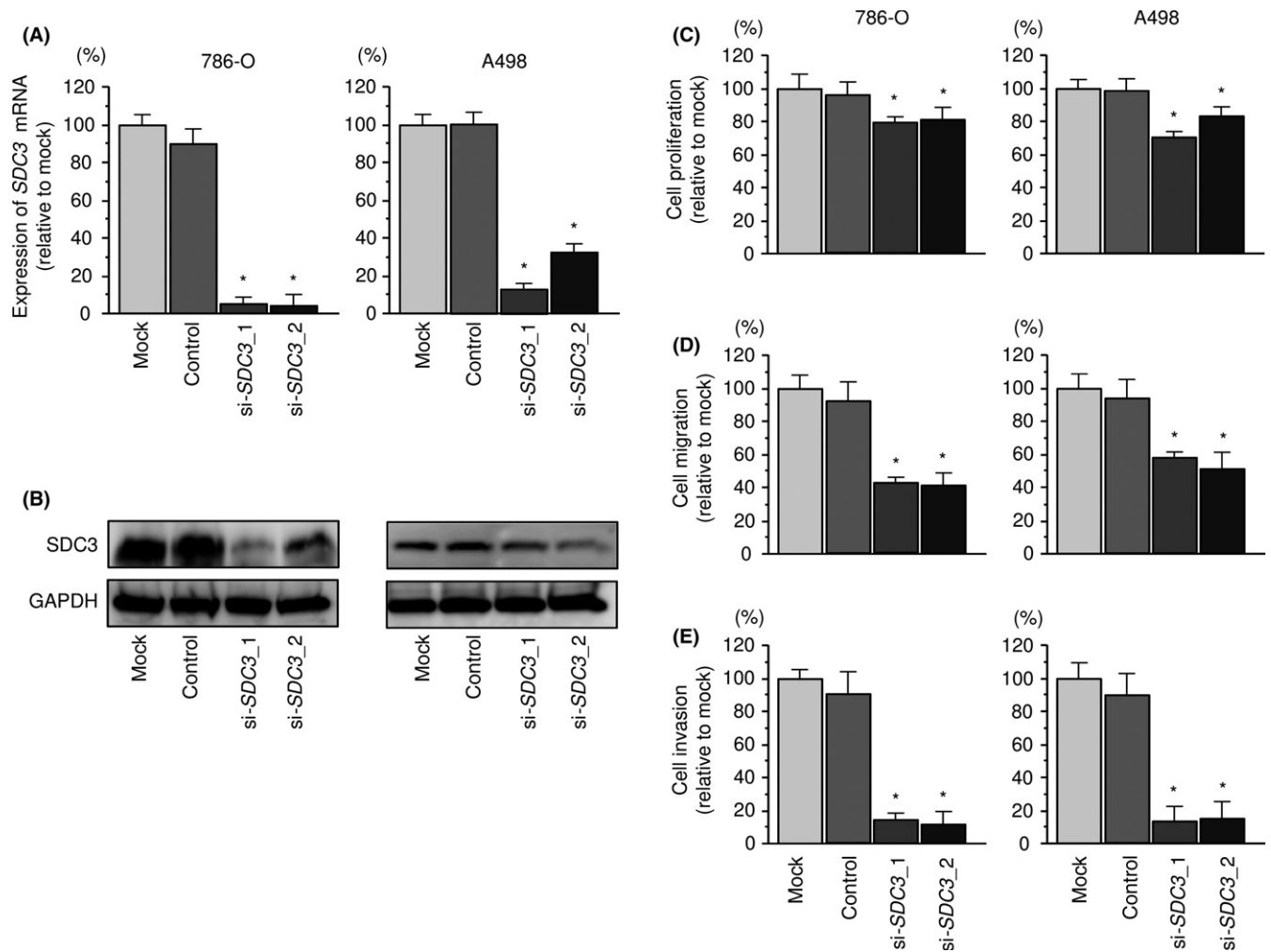
FIGURE 6 Effects of silencing *SDC3* in renal cell carcinoma cell lines. A, *SDC3* mRNA expression 72 hours after transfection with 10 nmol/L si-*SDC3*_1 or si-*SDC3*_2 into renal cell carcinoma cell lines. *GAPDH* was used as an internal control. B, Syndecan-3 (SDC3) protein expression 72 hours after transfection with si-*SDC3*_1 or si-*SDC3*_2. GAPDH was used as a loading control. C, Cell proliferation was determined with XTT assays 72 hours after transfection with 10 nmol/L si-*SDC3*_1 or si-*SDC3*_2. D, Cell migration activity was determined by migration assays. E, Cell invasion activity was determined using Matrigel invasion assays. *$P < .0001$

(Table 4), from which a gene expression heat map was constructed (Figure 8A). In the heat map, we focused on a gene cluster including *SDC3* (*IL18RAP*, *SDC3*, *SH2D1A*, *GZMH*, *KIF21B*, *TMC8*, *GAB3*, *HLA-DPB2*, *PLEK*, and *C1Qb*) (Figure 8B). Furthermore, patients with high gene signature expression (Figure 8B, red square) were significantly associated with a lower overall survival rate than those with low gene signature expression (Figure 8B, blue square) ($P = 0.0064$, Figure 8C). Furthermore, high expression of 7 genes (*SDC3*, *PLXDC1*, *IL18RAP*, *GZMH*, *ATP8B3*, *TBX15*, and *TMC8*) was significantly associated with poor prognosis of RCC patients by TCGA datasets (Figure S3).

3.9 | Analysis of pre-miR-144 and the SDC family in RCC pathogenesis and clinical outcome from TCGA database

Figure 9A shows that patients with high expression of *SDC3* had shorter disease-free survival. Furthermore, high expression of *SDC3*

was significantly associated with advanced tumor stage and high pathological grade (Figure 9B-F).

Conversely, low expression levels of *miR-144-5p* and *miR-144-3p* were significantly associated with shorter disease-free survival and advanced tumor stage (Figure S4).

The univariate and multivariate Cox proportional hazards model showed that high expression of *SDC3* was an independent predictive factor for survival (hazard ratio, 1.77; 95% confidence interval, 1.07-2.97; $P = 0.0249$), as were well-known clinical prognostic factors such as T stage, M stage, and hemoglobin level (Table 5).

In further analyses, we investigated the relationships between other genes in the syndecan family (*SDC1*, *SDC2*, and *SDC4*) and RCC pathogenesis. Interestingly, no other *SDC* family gene had a significant relationship between its expression and patient prognosis, tumor stage, or pathological grade in RCC (Figure S5).
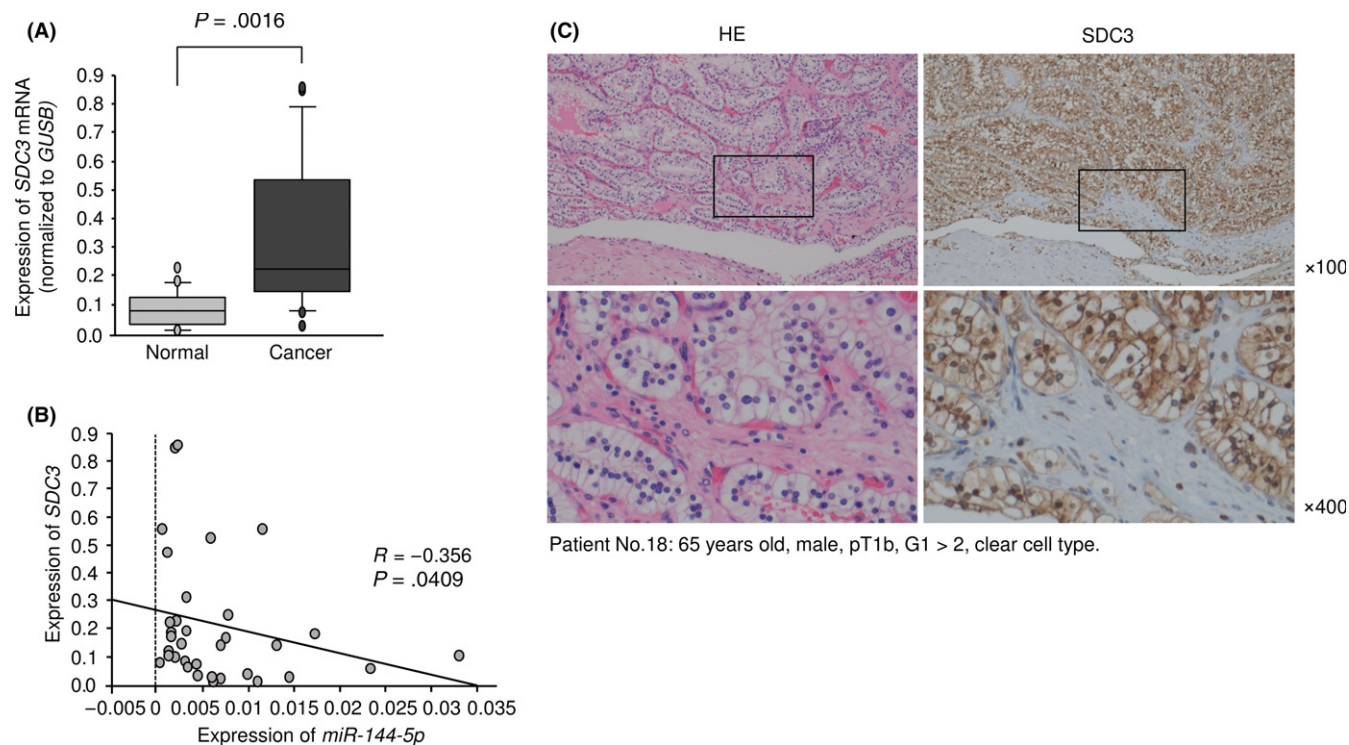
FIGURE 7 Expression of SDC3 in clinical specimens of renal cell carcinoma. A, Expression levels of *SDC3* in RCC clinical specimens. *GUSB* was used as an internal control. B, Spearman's rank test showed the negative correlation between *SDC3* expression and *miR-144-5p*. C, Immunostaining showed that SDC3 was strongly expressed in cancer lesions (100× and 400× magnification field)

3.10 | Effect of cotransfection of *SDC3/miR-144-5p* in 786-O cells

In order to investigate whether the *SDC3/miR-144-5p* axis is essential for RCC pathogenesis, we applied rescue studies in 786-O cells. Our present studies showed that cell proliferation, migration, and invasive abilities were recovered by cotransfection of *SDC3* expression vector and *miR-455-5p* mature miRNA compared to *miR-144-5p* transfection alone (Figure 10). These findings suggested that overexpression of *SDC3* contributed to aggressiveness of RCC cells.

A schema summarizing these results of the study is shown in Figure S6.

4 | DISCUSSION

The general understanding of miRNA biogenesis posits that only guide strands of miRNAs (derived from the miRNA duplex) are incorporated into the RISC and actually modulate target RNA transcripts.[25] Passenger strands of miRNAs are also thought to undergo degradation, becoming nonfunctional.[26] Contrary to this point of view, our miRNA signatures showed that some miRNA passenger strands were aberrantly expressed in several cancer tissues.[15,17] Our previous studies revealed that *miR-145-3p* (the passenger strand of the *miR-145* duplex) was significantly reduced in clinical specimens of prostate cancer as well as head and neck squamous cell carcinoma. Moreover, ectopic expression of *miR-145-3p* blocked cancer

cell aggressiveness, suggesting that the passenger strand of the *miR-145* duplex acts as an antitumor miRNA, as does *miR-145-5p* (the guide strand).[15,16] Moreover, *miR-145-3p* was incorporated into the RISC and targeted several oncogenes (eg *MELK*, *NCAPG*, *BUB1*, *CDK1*, and *MYO1B*) in cancer cells.[15,16] Importantly, these *miR-145-3p* targets were deeply involved in cancer pathogenesis. For example, high expression of *MELK*, *NCAPG*, *BUB1*, and *CDK1* significantly predicted survival in patients with prostate cancer.[15]

Some miRNAs are distributed in clusters on human chromosomes.[27] Analyses of our miRNA signature of RCC based on RNA sequencing showed that *miR-451a* was significantly downregulated in cancer tissues and it had antitumor functions.[13] In the human genome, *miR-451a*, *miR-451b*, *miR-4732*, *miR-144-5p*, and *miR-144-3p* form a miRNA cluster at 17q11.2. Among these miRNAs, low expression of *miR-451a*, *miR-144-5p*, and *miR-144-3p* predicted poor prognosis of patients with RCC according to TCGA database analyses. Our data showed that both strands of *miR-144-5p* and *miR-144-3p* had antitumor functions in RCC cells. Many studies have reported that *miR-144-3p* acted as an antitumor miRNA in several types of cancers.[28,29] In contrast to recent analyses of *miR-144-3p*, few papers have examined the function of *miR-144-5p* in cancer cells. We previously showed that *miR-144-5p* had tumor-suppressive functions through its targeting of *CCNE1* and *CCNE2* in bladder cancer.[18] It is very interesting that members of this miRNA cluster at 17q11.2 have cancer-suppressing effects. These results suggest that the anticancer effects of this miRNA cluster should be closely examined in many cancers.

**TABLE 4** Candidate downstream genes of *SDC3* in renal cell carcinoma cells

Gene symbol	Gene name	Log$_2$ (si-*SDC3*_1/mock)	Log$_2$ (si-*SDC3*_2/mock)	Average Log$_2$ (si-*SDC3*/mock)	GEO expression data fold change (tumor/normal)	Cytoband	TCGA data OS (*P*-value)
SDC3	Syndecan 3	−2.319	−2.821	−2.570	2.432	hs|1p35.2	0.000271
GAB3	GRB2-associated binding protein 3	−1.599	−1.879	−1.739	2.467	hs|Xq28	0.200000
PLXDC1	Plexin domain containing 1	−0.481	−2.365	−1.423	3.144	hs|17q12	0.001860
SH2D1A	SH2 domain containing 1A	−1.092	−1.692	−1.392	2.214	hs|Xq25	0.133000
SFMBT2	Scm-like with four mbt domains 2	−1.240	−1.434	−1.337	2.189	hs|10p14	0.009770[a]
NFATC2	Nuclear factor of activated T cells, cytoplasmic, calcineurin-dependent 2	−1.036	−1.624	−1.330	2.259	hs|20q13.2	0.002260[a]
KIF21B	Kinesin family member 21B	−1.385	−1.231	−1.308	2.701	hs|1q32.1	0.148000
NLGN1	Neuroligin 1	−0.971	−1.518	−1.244	2.423	hs|3q26.31	0.039100[a]
PREX2	Phosphatidylinositol-3,4,5-trisphosphate-dependent Rac exchange factor 2	−1.088	−1.390	−1.239	2.213	hs|8q13.2	0.069000
CALHM2	Calcium homeostasis modulator 2	−1.858	−0.617	−1.237	2.940	hs|10q24.33	0.135000
IL18RAP	Interleukin 18 receptor accessory protein	−0.431	−1.976	−1.203	3.967	hs|2q12.1	0.001070
PLEK	Pleckstrin	−1.275	−1.123	−1.199	3.395	hs|2p13.3	0.121000
PECAM1	Platelet/endothelial cell adhesion molecule 1	−0.465	−1.931	−1.198	2.831	hs|17q23.3	0.036500[a]
ZNF660	Zinc finger protein 660	−0.452	−1.913	−1.183	2.274	hs|3p21.31	0.155000
ELTD1	EGF, latrophilin, and seven transmembrane domain containing 1	−0.634	−1.612	−1.123	2.297	hs|1p31.1	No data
KCNJ8	Potassium channel, inwardly rectifying subfamily J, member 8	−0.465	−1.720	−1.093	2.002	hs|12p12.1	0.495000
ITGA4	Integrin, alpha 4 (antigen CD49D, alpha 4 subunit of VLA-4 receptor)	−0.369	−1.788	−1.079	2.336	hs|2q31.3	0.573000
GZMH	Granzyme H (cathepsin G-like 2, protein h-CCPX)	−0.273	−1.882	−1.077	5.323	hs|14q12	0.012900
ATP8B3	ATPase, aminophospholipid transporter, class I, type 8B, member 3	−0.470	−1.647	−1.059	2.941	hs|19p13.3	7.35E-07
ZG16B	Zymogen granule protein 16B	−1.156	−0.955	−1.056	2.080	hs|16p13.3	0.596000
HLA-DPB2	Major histocompatibility complex, class II, DP beta 2 (pseudogene)	−0.988	−1.111	−1.050	3.123	hs|6p21.32	0.968000
TBX15	T-box 15	−0.442	−1.631	−1.036	4.119	hs|1p12	0.001930
C1QB	Complement component 1, q subcomponent, B chain	−1.363	−0.661	−1.012	6.547	hs|1p36.12	0.070700
TMC8	Transmembrane channel-like 8	−0.651	−1.370	−1.011	2.786	hs|17q25.3	0.001460
SLITRK5	SLIT and NTRK-like family, member 5	−1.372	−0.636	−1.004	5.478	hs|13q31.2	0.016200[a]
HECW2	HECT, C2, and WW domain containing E3 ubiquitin protein ligase 2	−0.984	−1.017	−1.000	2.663	hs|2q32.3	0.000152[a]

[a]Poor prognosis with low expression.
GEO, Gene Expression Omnibus; OS, overall survival; TCGA, The Cancer Genome Atlas.

In miRNA-based cancer research, elucidation of target genes and RNA networks controlled by aberrantly expressed miRNAs is an important approach to better understanding the development and progression of tumors. In this study, we identified 65 putative targets of *miR-144-5p* regulation in RCC cells. Among these targets, high expression of 9 genes (*FAM64A*, *F2*, *TRIP13*, *ANKRD36*, *CENPF*, *NCAPG*, *CLEC2D*, *SDC3*, and *SEMA4B*) significantly predicted poor survival in patients with RCC (*P* < .001), suggesting they might be good prognostic markers. Among them, coagulation factor 2 (*F2*), which was overexpressed in advanced RCC, is related to tumor progression in several types of cancers.[30] Furthermore, centromere protein F (*CENPF*) was previously reported to be regulated by antitumor *miR-205* and involved in prostate cancer pathogenesis.[31] Non-SMC condensin I complex, subunit G (*NCAPG*) was also directly regulated
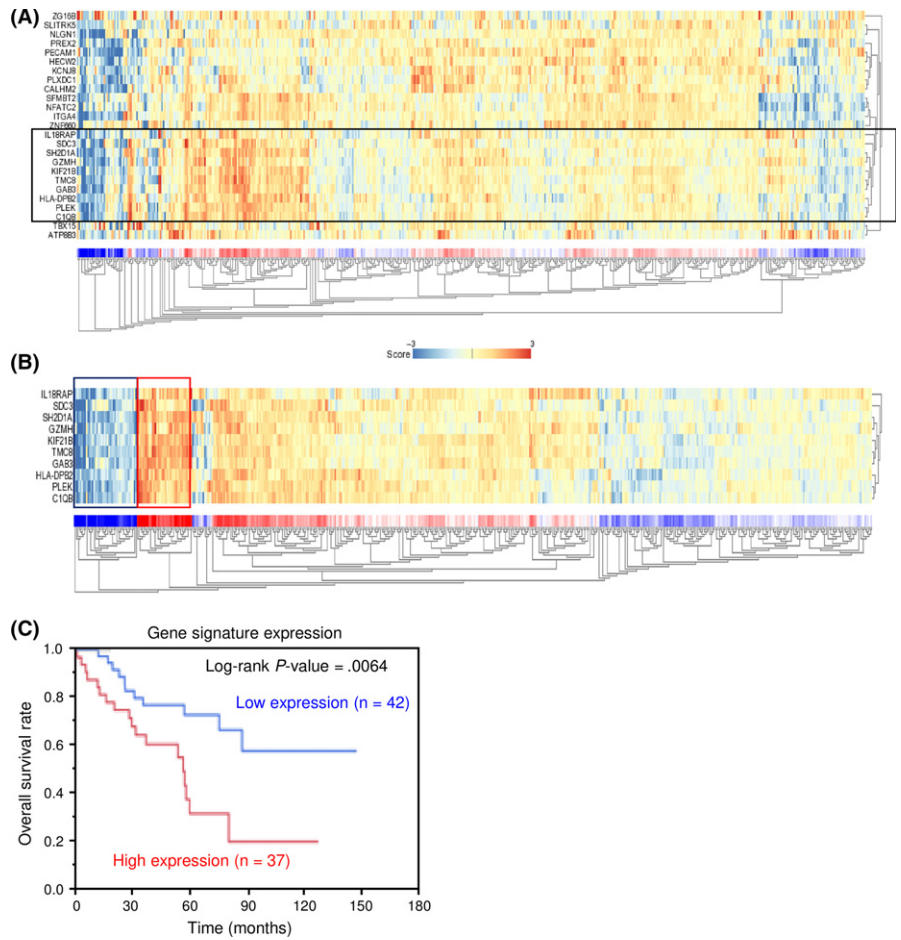
FIGURE 8 Heat map showing gene expression and Kaplan-Meier analysis in renal cell carcinoma cells. A, Heat map visualization of candidate genes downstream from SDC3. B, Heat map visualization of a gene signature including SDC3 (black square). C, Kaplan-Meier analysis of overall survival of patients with high gene signature expression (red square) and those with a low gene signature expression (blue square)
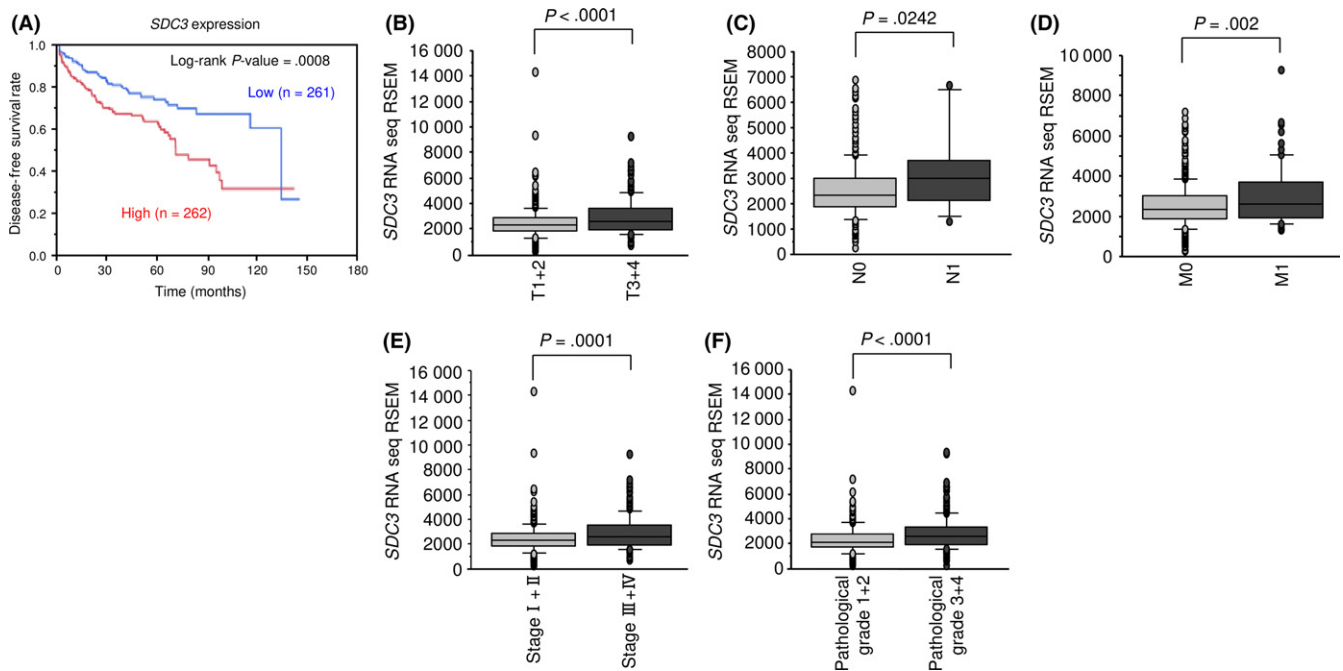
FIGURE 9 The Cancer Genome Atlas database analysis of SDC3 in renal cell carcinoma. A, Patients with high SDC3 expression had shorter disease-free survival than those with low expression. B-F, High SDC3 expression was significantly associated with advanced tumor stage and pathological grade

**TABLE 5** Univariable and multivariable Cox hazard regression models for overall survival in renal cell carcinoma

Variable	Group	Univariable			Multivariable		
		HR	95% CI	P-value	HR	95% CI	P-value
SDC3 expression	High/low	1.73	1.28-2.36	0.0003	1.77	1.07-2.97	0.0249
Age, years	≥60/<60	1.84	1.35-2.54	0.0001	1.51	0.91-2.57	0.1131
Gender	Male/female	0.97	0.72-1.34	0.8684	–	–	–
T stage	3 + 4/1 + 2	3.05	2.26-4.14	<0.0001	2.94	1.05-10.44	0.0381
N stage	Positive/negative	3.07	1.49-5.65	0.0038	0.66	0.19-1.95	0.4708
M stage	Positive/negative	4.27	3.11-5.82	<0.0001	5.11	2.57-10.07	<0.0001
Stage	III + IV/I + II	3.72	2.72-5.13	<0.0001	0.55	0.14-1.82	0.3423
Histological grade	G3 + 4/G1 + 2	2.59	1.86-3.68	<0.0001	1.06	0.62-1.86	0.8232
Serum Ca level	High/normal	4.38	2.06-8.18	0.0005	0.74	0.19-2.33	0.6173
Serum Hb level	Low/normal	2.13	1.52-3.05	<0.0001	1.67	1.00-2.89	0.0488

–, not included in analysis. Ca, calcium; CI, confidence interval; Hb, hemoglobin; HR, hazard ratio.

by miR-145-3p and associated with tumor development in prostate cancer.[15]

In the present study, we focused on SDC3 as a crucial oncogene directly regulated by miR-144-5p in RCC cells. The syndecan protein family consists of four transmembrane proteoglycans in mammals (SDC1-4). In carcinogenesis, syndecans, integrins, and growth factor receptors interact and play important roles in cell signaling. They appear to be involved in both cancer initiation and progression.[32]
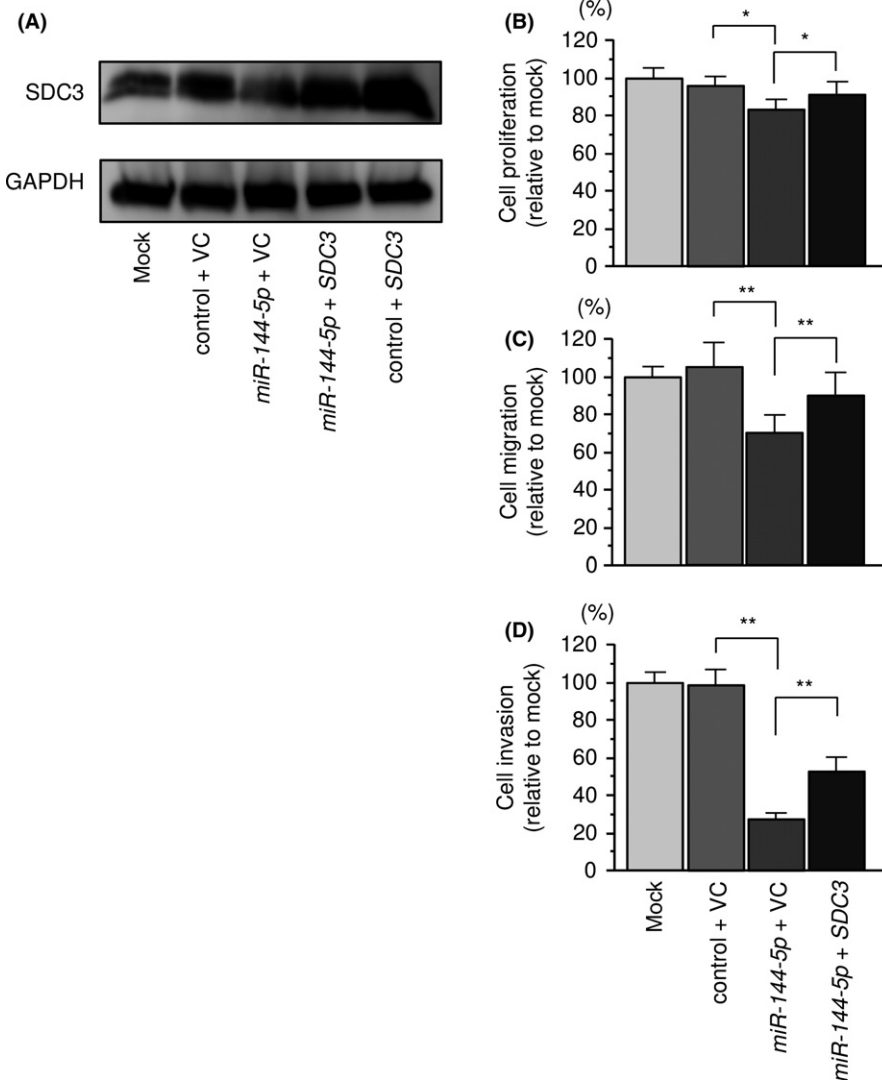
FIGURE 10 Effects of cotransfection of SDC3/miR-144-5p into 786-O cells. A, Syndecan-3 (SDC3) protein expression was evaluated by Western blot analysis of 786-O cells. The rescue studies were evaluated 48 hours after reverse transfection with miR-144-5p and 24 hours after forward transfection with the SDC3 vector. GAPDH was used as a loading control. B, Cell proliferation was determined using XTT assays 72 hours after reverse transfection with miR-144-5p and 48 hours after forward transfection with the SDC3 vector. C, Cell migration activity was assessed by wound healing assays 48 hours after reverse transfection with miR-144-5p and 24 hours after forward transfection with the SDC3 vector. D, Cell invasive activity was evaluated by invasion assays 48 hours after reverse transfection with miR-144-5p and 24 hours after forward transfection with SDC3 vector. *$P < .005$, **$P < .0001$. VC, vector control

Although they are similar in molecular structure, it has been reported that their expression and biological roles in cancer cells are different. Relatively little is known about *SDC3*, whereas *SDC1*, *SDC2*, and *SDC4* have been shown to possess oncogenic functions in several types of cancers.[33-35] *SDC3* is primarily expressed in nerve tissue and developed musculoskeletal tissues. Overexpression of the gene might be involved in perineural invasion and shorter survival in pancreatic cancer.[32] *SDC3* and perlecan were particularly strongly expressed in tumor stromal vessels, indicating that these heparan sulfate proteoglycans play pivotal roles in tumor angiogenesis.[32] Furthermore, the SDC3-mediated signaling pathway might lead to prostate cancer cell migration, invasion, and metastasis.[32] These findings indicate that *SDC3* expression could be associated with RCC progression.

Furthermore, we identified a gene signature of *SDC3* downstream and its expressions were significantly related to cancer aggressiveness. Among 26 downstream genes, several genes have already reported roles in RCC pathogenesis. *ITGA4* promoted cancer cell metastasis and the kinesin family was related to cell proliferation, invasion, and migration in RCC.[36,37] Interestingly, high expression of 7 genes (*SDC3*, *PLXDC1*, *IL18RAP*, *GZMH*, *ATP8B3*, *TBX15*, and *TMC8*) significantly predicted poor prognosis of RCC patients according to TCGA datasets. *PLXDC1* (also known as *TEM7*) was initially cloned as a high expression protein from vascular endothelium of human cancer.[38] Several studies showed that its expression contributed to angiogenesis.[39,40] In gastric cancer, aberrant expression of *PLXDC1* enhanced cancer cell migration and invasive abilities.[41] *TBX15* is a member of the T-box family of transcription factors; dysregulated expression of some *TBX* members is involved in human disease and carcinogenesis.[42] In thyroid cancer cells, expression of *TBX15* induced Bcl2 and Bcl-XL (anti-apoptotic proteins) expression and its overexpression played a role of anti-apoptosis.[43] These studies showed that *SDC3* and its regulatory network have potential to be therapeutic targets of RCC. Further analysis of *SDC3* could contribute to the development of novel therapeutic strategies for RCC.[44]

In conclusion, we showed that the expression of both *miR-144-5p* and *miR-144-3p* was significantly downregulated in RCC tissues and that they functioned as tumor suppressors in RCC cells. We found that *SDC3* was directly regulated by *miR-144-5p* and that it is a significant gene in RCC pathogenesis. Overexpression of *SDC3* was involved in the pathogenesis of RCC and acted as an oncogene. The antitumor functionality of the passenger strand of miRNA is a new concept in cancer research. Searching for RNA networks controlled by passenger strands of miRNA is a new challenge in studies of RCC pathogenesis.

CONFLICT OF INTEREST

The authors declare no conflict of interest.

ORCID

Yasutaka Yamada http://orcid.org/0000-0002-0070-1590
Takayuki Arai http://orcid.org/0000-0002-3888-9576

REFERENCES

1. Capitanio U, Montorsi F. Renal cancer. *Lancet*. 2016;387 (10021):894-906.
2. Ljungberg B, Campbell SC, Choi HY, et al. The epidemiology of renal cell carcinoma. *Eur Urol*. 2011;60(4):615-621.
3. Gupta K, Miller JD, Li JZ, Russell MW, Charbonneau C. Epidemiologic and socioeconomic burden of metastatic renal cell carcinoma (mRCC): a literature review. *Cancer Treat Rev*. 2008;34(3):193-205.
4. Figlin R, Sternberg C, Wood CG. Novel agents and approaches for advanced renal cell carcinoma. *J Urol*. 2012;188(3):707-715.
5. Goto Y, Kurozumi A, Enokida H, Ichikawa T, Seki N. Functional significance of aberrantly expressed microRNAs in prostate cancer. *Int J Urol*. 2015;22(3):242-252.
6. Hayes J, Peruzzi PP, Lawler S. MicroRNAs in cancer: biomarkers, functions and therapy. *Trends Mol Med*. 2014;20(8):460-469.
7. Kurozumi A, Goto Y, Okato A, Ichikawa T, Seki N. Aberrantly expressed microRNAs in bladder cancer and renal cell carcinoma. *J Hum Genet*. 2017;62(1):49-56.
8. Koshizuka K, Hanazawa T, Fukumoto I, Kikkawa N, Okamoto Y, Seki N. The microRNA signatures: aberrantly expressed microRNAs in head and neck squamous cell carcinoma. *J Hum Genet*. 2017;62(1):3-13.
9. Arai T, Okato A, Kojima S, et al. Regulation of spindle and kinetochore-associated protein 1 by antitumor miR-10a-5p in renal cell carcinoma. *Cancer Sci*. 2017;108(10):2088-2101.
10. Nishikawa R, Goto Y, Kojima S, et al. Tumor-suppressive microRNA-29s inhibit cancer cell migration and invasion via targeting LAMC1 in prostate cancer. *Int J Oncol*. 2014;45(1):401-410.
11. Goto Y, Kurozumi A, Nohata N, et al. The microRNA signature of patients with sunitinib failure: regulation of UHRF1 pathways by microRNA-101 in renal cell carcinoma. *Oncotarget*. 2016;7 (37):59070-59086.
12. Okato A, Arai T, Yamada Y, et al. Dual strands of Pre-miR-149 inhibit cancer cell migration and invasion through targeting FOXM1 in renal cell carcinoma. *Int J Mol Sci*. 2017;18(9).
13. Yamada Y, Arai T, Sugawara S, et al. Impact of novel oncogenic pathways regulated by anti-tumor miR-451a in renal cell carcinoma. *Cancer Sci*. 2018;109(4):1239-1253.
14. Yonemori M, Seki N, Yoshino H, et al. Dual tumor-suppressors miR-139-5p and miR-139-3p targeting matrix metalloprotease 11 in bladder cancer. *Cancer Sci*. 2016;107(9):1233-1242.
15. Goto Y, Kurozumi A, Arai T, et al. Impact of novel miR-145-3p regulatory networks on survival in patients with castration-resistant prostate cancer. *Br J Cancer*. 2017;117(3):409-420.
16. Yamada Y, Koshizuka K, Hanazawa T, et al. Passenger strand of miR-145-3p acts as a tumor-suppressor by targeting MYO1B in head and neck squamous cell carcinoma. *Int J Oncol*. 2018;52(1):166-178.
17. Koshizuka K, Nohata N, Hanazawa T, et al. Deep sequencing-based microRNA expression signatures in head and neck squamous cell carcinoma: dual strands of pre-miR-150 as antitumor miRNAs. *Oncotarget*. 2017;8(18):30288-30304.

18. Matsushita R, Seki N, Chiyomaru T, et al. Tumour-suppressive micro-RNA-144-5p directly targets CCNE1/2 as potential prognostic markers in bladder cancer. *Br J Cancer*. 2015;113(2):282-289.

19. Koshizuka K, Hanazawa T, Kikkawa N, et al. Regulation of ITGA3 by the anti-tumor miR-199 family inhibits cancer cell migration and invasion in head and neck cancer. *Cancer Sci*. 2017;108(8):1681-1692.

20. Nishikawa R, Chiyomaru T, Enokida H, et al. Tumour-suppressive microRNA-29s directly regulate LOXL2 expression and inhibit cancer cell migration and invasion in renal cell carcinoma. *FEBS Lett*. 2015;589(16):2136-2145.

21. R2: genomics analysis and visualization platform. http://r2.amc.nl. Accessed March 9, 2018.

22. J A. OncoLnc: linking TCGA survival data to mRNAs, miRNAs, and lncRNAs. *PeerJ Comput Sci*. 2016;2:e67.

23. Gao J, Aksoy BA, Dogrusoz U, et al. Integrative analysis of complex cancer genomics and clinical profiles using the cBioPortal. *Sci Signal*. 2013;6(269):pl1.

24. Cerami E, Gao J, Dogrusoz U, et al. The cBio cancer genomics portal: an open platform for exploring multidimensional cancer genomics data. *Cancer Discov*. 2012;2(5):401-404.

25. Gregory RI, Chendrimada TP, Cooch N, Shiekhattar R. Human RISC couples microRNA biogenesis and posttranscriptional gene silencing. *Cell*. 2005;123(4):631-640.

26. Matranga C, Tomari Y, Shin C, Bartel DP, Zamore PD. Passenger-strand cleavage facilitates assembly of siRNA into Ago2-containing RNAi enzyme complexes. *Cell*. 2005;123(4):607-620.

27. Chhabra R, Dubey R, Saini N. Cooperative and individualistic functions of the microRNAs in the miR-23a~27a~24-2 cluster and its implication in human diseases. *Mol Cancer*. 2010;9:232.

28. Gao Z, Liu R, Liao J, et al. Possible tumor suppressive role of the miR-144/451 cluster in esophageal carcinoma as determined by principal component regression analysis. *Mol Med Rep*. 2016;14(4):3805-3813.

29. Zhang SY, Lu ZM, Lin YF, et al. miR-144-3p, a tumor suppressive microRNA targeting ETS-1 in laryngeal squamous cell carcinoma. *Oncotarget*. 2016;7(10):11637-11650.

30. John A, Gorzelanny C, Bauer AT, Schneider SW, Bolenz C. Role of the coagulation system in genitourinary cancers: review. *Clin Genitourin Cancer*. 2017;16(1):e29-e39.

31. Nishikawa R, Goto Y, Kurozumi A, et al. MicroRNA-205 inhibits cancer cell migration and invasion via modulation of centromere protein F regulating pathways in prostate cancer. *Int J Urol*. 2015;22(9):867-877.

32. Afratis NA, Nikitovic D, Multhaupt HA, Theocharis AD, Couchman JR, Karamanos NK. Syndecans - key regulators of cell signaling and biological functions. *FEBS J*. 2017;284(1):27-41.

33. Szatmari T, Otvos R, Hjerpe A, Dobra K. Syndecan-1 in cancer: implications for cell signaling, differentiation, and prognostication. *Dis Markers*. 2015;2015:796052.

34. Kousidou O, Berdiaki A, Kletsas D, et al. Estradiol-estrogen receptor: a key interplay of the expression of syndecan-2 and metalloproteinase-9 in breast cancer cells. *Mol Oncol*. 2008;2(3):223-232.

35. Saoncella S, Echtermeyer F, Denhez F, et al. Syndecan-4 signals cooperatively with integrins in a Rho-dependent manner in the assembly of focal adhesions and actin stress fibers. *Proc Natl Acad Sci USA*. 1999;96(6):2805-2810.

36. Markovic-Lipkovski J, Brasanac D, Muller GA, Muller CA. Cadherins and integrins in renal cell carcinoma: an immunohistochemical study. *Tumori*. 2001;87(3):173-178.

37. Li G, Chong T, Yang J, Li H, Chen H. Kinesin motor protein KIFC1 is a target protein of miR-338-3p and associated with poor prognosis and progression of renal cell carcinoma. *Oncol Res*. 2018; https://doi.org/10.3727/096504018X15213115046567.

38. St Croix B, Rago C, Velculescu V, et al. Genes expressed in human tumor endothelium. *Science*. 2000;289(5482):1197-1202.

39. Yamaji Y, Yoshida S, Ishikawa K, et al. TEM7 (PLXDC1) in neovascular endothelial cells of fibrovascular membranes from patients with proliferative diabetic retinopathy. *Invest Ophthalmol Vis Sci*. 2008;49(7):3151-3157.

40. Bagley RG, Rouleau C, Weber W, et al. Tumor endothelial marker 7 (TEM-7): a novel target for antiangiogenic therapy. *Microvasc Res*. 2011;82(3):253-262.

41. Zhang ZZ, Hua R, Zhang JF, et al. TEM7 (PLXDC1), a key prognostic predictor for resectable gastric cancer, promotes cancer cell migration and invasion. *Am J Cancer Res*. 2015;5(2):772-781.

42. Peres J, Davis E, Mowla S, et al. The highly homologous T-Box transcription factors, TBX2 and TBX3, have distinct roles in the oncogenic process. *Genes Cancer*. 2010;1(3):272-282.

43. Arribas J, Gimenez E, Marcos R, Velazquez A. Novel antiapoptotic effect of TBX15: overexpression of TBX15 reduces apoptosis in cancer cells. *Apoptosis*. 2015;20(10):1338-1346.

44. Rhee J, Hoff PM. Angiogenesis inhibitors in the treatment of cancer. *Expert Opin Pharmacother*. 2005;6(10):1701-1711.

SUPPORTING INFORMATION

Additional supporting information may be found online in the Supporting Information section at the end of the article.